De-alloying Kinetics of an Au-based Amorphous Alloy

Federico Scaglione, Paola Rizzi, Livio Battezzati
Journal of Alloys and Compounds 536S (2012) S60– S64
doi:10.1016/j.jallcom.2011.11.087

Journal of Alloys and Compounds 536S (2012) S60– S64

De-alloying kinetics of an Au-based amorphous alloys

Federico Scaglione, Paola Rizzi, Livio Battezzati∗
Dipartimento di Chimica IFM e Centro NIS, Università di Torino, Via P. Giuria 7, 10125 Torino, Italy

Abstract
The process of de-alloying, i.e. removal of a less noble metal from an alloy, is applied here by electrochemical means to a Au-based metallic glass, Au40Cu28Ag7Pd5Si20, as a function of potential, temperature, and time. Very fine crystals nucleate with random orientation at the solid–electrolyte interface forming ligaments. The resulting material is constituted by ligaments made of pure Au and pores of smaller size whose dimensions coarsen up as a function of time to slightly above two hundred and below one hundred nanometers, respectively. The microstructure is uniform on both surfaces and across the ribbon. The extent of de-alloying is measured by monitoring the heat of crystallisation of the remaining amorphous phase giving linear trend vs time suggesting the reactions occur on continuously renewed surfaces.

1. Introduction

Porous metals are of interest for in various field such as catalysis, sensors, hydrogen storage, molecular sieves. They can be produced by de-alloying of crystalline homogeneous solid solutions, most often based on noble metals, i.e. selective removal of a phase or an element from a bulk alloy by chemical or electrochemical means resulting in the formation of a network of pores and ligaments of the remaining noble element [1]. This process has been dealt with in a number of works, most of them involving binary systems, especially Au–Cu, and Au–Ag [2–4]. For successful de-alloying a substantial difference in electrochemical potential between alloy components is needed. Formation of porous structures occurs at a critical potential and below the “parting limit”, i.e. the maximum content of the most noble element at which interconnected porosity is formed. Once the less noble element is removed, the noble element atoms reorganise themselves by surface diffusion forming hillocks separated by pores [1]. The process is then repeated throughout the thickness of the specimen. The original grains are retained and in each of them the network of ligaments constitutes a single crystals made of fine domains having an angular difference of a few degree between each other [5]. With this evidence for homogeneous crystalline solid solutions, it is of interest to investigate how de-alloying occurs in amorphous alloys. De-alloying of homogeneous amorphous alloys as well as of phase separated amorphous phases, has been attempted in a number of cases with success [6–11]. Amorphous alloys contain often several components, therefore all elements but one are removed at an appropriate potential. It has been shown that porous metals are obtained similarly to crystalline alloys. However, the de-alloying mechanism has not been studied in detail yet. It is expected that nucleation of a crystalline phase occurs since the removal of elements will shift the composition outside the glassforming range. In previous works with quaternary Au–Cu–Ti–Si alloys [10,11], the morphology of the surface and its homogeneity appeared as key parameters in de-alloying. The air-side of the ribbon was smoother but not chemically homogeneous in that it contained embedded fine crystals. Here, the removal of the crystalline phase provided centres for preferential etching. The wheel side was more chemically homogeneous, but rough. Again the etching appeared favoured on surface asperities. In this work we study electrochemical de-alloying using a Au-based alloy which is good glass former with the

aim of elucidating aspects of the de-alloying kinetics and of producing substantial quantities of porous material in the form of ribbon.

2. Experimental

The Au40Cu28Ag7Pd5Si20 alloy has been chosen for the experiments because of its reported good glass forming tendency combined with an Au content below the usual parting limit found for Au alloys [12]. Ingots were prepared by arc-melting the pure elements (Au: 99.99%, Ag, Cu and Pd: 99.99%, Si: 99.9995%) in Ar atmosphere and using Ti getters. Ribbons about 25 □m thick and 2 mm wide were obtained by melt spinning with a linear velocity of the copper wheel of 22 m/s. Samples of 15 mm in length were cut from ribbons. For electrochemical de-alloying, samples have been used as working electrode in a cell composed of either a Standard Calomel reference electrode (SCE) or an Ag/AgCl electrode and a Pt counter electrode in a Potentiostat/Galvanostat Model 7050, Amel Instruments. A double bridge configuration has been employed to avoiddeposition of the de-alloyed ions as insoluble salts. The critical potential for dealloying Ec has been determined by performing anodic polarisation experiments [13]. The de-alloying behaviour of alloys has been investigated using potentiostatic method in an electrolyte made of a 1 M HNO3 aqueous solution. Samples have been etched for various amounts of time at 1.05 V (vs the Ag/AgCl electrode). The alloy has been analysed before and after etching using X-ray diffraction (XRD) in Bragg–Brentano geometry with monochromatic Cu K□ radiation, scanning electron microscopy (SEM), Energy Dispersive X-ray Spectroscopy (EDS) (calibrated with a pure Co sample), High Resolution Transmission Electron Microscopy (HRTEM), Differential Scanning Calorimetry (DSC) at the heating rate of 20 K/min. 3. Results and discussion

3.1. Alloy characterisation and electrochemical details

The Au40Cu28Ag7Pd5Si20 alloy under consideration resulted fully amorphous to XRD after rapid solidification (pattern in Fig. 1) and TEM (Fig. 2a). Occasional dendritic crystals some tens of nanometer in size occurred in the ribbon and could be imaged by TEM (not shown) as well as a few quenched-in fine crystals, one example being seen in the selected area of Fig. 2a. The glass transition is found at 411 K and the crystallisation takes place at 443 K in agreement with the values first given in [12]. A DSC trace is shown in Fig. 3. Polarisation curves at increasing temperatures are shown in Fig. 4. At room temperature the curve exhibits two minima at 0.21 and 0.55 V and generally a reduced active dissolution due to a passivation region extended from 0.9 to 1.6 V with a very low passive current density of 10−5 A/cm2; than the currentdensity increases abruptly at high values. The increase in temperature involves the increase of the current density in the whole range of potentials: in the anodic region of the curve, an active region at about 1 V vs SCE is noticed, followed by a passivation region before transpassive current increase. The critical potential for stable de-alloying was found in the 1 V region where an anodic current density of the order of 10−3 A/cm2 has been measured. The critical potential vs the Ag/AgCl reference electrode has been evaluated in 1.05 V. The first minimum in the polarisation curve can be attributed to oxidation of nitrogen species that are formed in the cathodic region of the curve: indeed this signal is not present if the experiment is performed in 1 N H2SO4 solution [12]; the second minimum occurs at the corrosion potential of the alloy in fact the Open Circuit Voltage approaches this value. Since it is aimed at obtaining full de-alloying, the operative potential has been set above the second minimum. De-alloying at higher potential resulted in pronounced corrosion cracking of the alloy at all temperatures. This is at variance to a previous work on Au42Cu29Ti8Si21 and Au42Cu29Ti8Si21 alloys which could be de-alloyed only at 1.75 V, although with more difficulty, because of the more passive behaviour of these alloys [10,11]. The de-alloying was performed at 343 K to increase the rate of etching, i.e. having a current density close to 1 mA/cm2. The current resulting from a typical potentiostatic experiment as a function of time is reported in Fig. 5. The current first increases to over 1 mA/cm2 and then stabilises for a substantial amount of time during etching of the larger part

of the volume of the ribbon (see kinetics below). Finally, it decreases steadily when most of the ribbon has been de-alloyed.

3.2. Microstructure of de-alloyed samples

The de-alloying occurs uniformly under the conditions specified above on both sides of the ribbon in spite of their morphological difference. Fig. 6 shows the surface microstructure after de-alloying for 600 s and 10,800 s. This is again different from the findings with Au42Cu29Ti8Si21 and Au42Cu29Ti8Si21 alloys which contained a fraction of a crystalline phase which was removed in advance of massive de-alloying especially from the air side of the ribbon. Also, the higher applied potential favoured de-alloying on surface roughness [10,11]. In the image of Fig. 6b taken on the ribbon wheel side, the roughness due to the surface finish of the wheel is still apparent as a shiny vertical feature which, however, is crossed by ligaments and pores of the same shape and size as elsewhere. Fig. 1 reports a series of XRD patterns of the surface as a function of time. These clearly show that the developing crystalline phase is face centred cubic. The lattice constants obtained at all times indicate it is always constituted by pure Au within the experimental error. Systematic EDS analyses confirm this result. The crystalline phase is made of interconnected particles separated by porous channels. The size of both particles and pores increases with time. Fig. 7 shows that the coarsening of pores and ligaments occurs mostly in the early stages of the process, i.e. within about 1800 s at the temperature of 70 ◦C, the size becoming then practically constant for longer times. The surface area, determined by BET at this stage is below 10 m2/g. At short times the Au crystalsare extremely fine. Fig. 2b shows a HRTEM image taken on the edge of a thin ribbon de-alloyed for 60 s where the crystalline domains are of the order of 2–8 nm in size while other areas of similar size display amorphous contrast. The crystals appear randomly oriented after copious nucleation. Rietveld analyses [14] of samples de-alloyed for 300, 1800, 3600 and 21,600 s suggest the scattering domains range from 26 to 57 nm irrespective of the time. The root mean square of the microstrain is of the order of (1–2) × 10−3. It is then deduced that ligaments are composed of several domains at all times. It is apparent that after nucleation crystals coarsen to some extent, but then they remain in the tens of nanometer range when ligaments coarsening occurs. This might indicate that lattice defects are incorporated in the ligaments as well as diffusing Au atoms. These results must be taken with caution because only a thin surface layer contribute to the XRD intensity and the crystals might display a distribution of sizes; a further source of scatter could be due to quenched-in crystals which will contribute to the scattered intensity. Analysing different parts of the ribbon occasional dendritic crystals were found at random giving textured reflections. After long de-alloying times the material becomes in this respect rather similar to those obtained by de-alloying crystalline solid solution [1,5]. There is, however, a major difference: crystal nucleate at random from the amorphous alloy whereas the original grain structure of the solid solution is preserved in the other case where the scattering domains differ of a small angular difference [5]. This suggests that the microstructure of the porous Au can be tailored by using different starting alloys, either amorphous and crystalline, using the appropriate processing parameters: potential, temperature, time.

3.3. De-alloying kinetics

On continued etching, the amorphous ribbon is progressively depleted of less noble metals almost to its entire thickness giving bulk porous materials. Cross sections of ribbons after partial (14,400 s) and full de-alloying (21,600 s) are shown in Fig. 8. A uniform porous microstructure is recognised on both sides showing that the electrolyte reaches continuously the interface through the pores. In Fig. 8a the surface fracture of the remaining amorphous layer is still clearly seen, whereas only a thin layer remains in the sample imaged in Fig. 8b. The de-alloyed thickness is seen to increase as a function of time (Fig. 9). The measurement of it, however, is strongly affected by the fact that the

samples were cut at random in a limited number of places and also by inevitable damages to the de-alloyed layer when operating with a scalpel. In order to have a more precise measure of the de-alloyed fraction, it has been devised to determine the heat of crystallisation of the remaining amorphous phase and relate it to that of the as-spun ribbon. Fig. 9 reports these data as well. The increase in de-alloyed fraction is apparently linear up to almost 80 percent at 10,800 s and then stops or increases very slowly. It should be remembered that the thickness of ribbons is not strictly constant because of surface roughness and waves, therefore it is likely that some thicker parts will de-alloy more slowly when the neighbouring zone are fully porous and the electrolyte will flow through them. The DSC traces of Fig. 3 reveal that the glass transition and the main crystallisation event occur at the same temperature irrespective of the de-alloying time. This suggests that the bulk of the amorphous phase does not change composition and structure during the etching. When the phase is electrochemically decomposed at the interface with the electrolyte, the noble metal atoms diffuse through the surface to either cluster in new nuclei or cause growth of already existing crystals. The transformations occurring after crystallisation at higher temperature are modified instead. It is likely that the crystallising phases react with the Au in contact with them to approach an equilibrium and this effect is detectable only when the amount of them is strongly reduced. In analogy with the general kinetics of interfacial processes, e.g. constant oxidation rate, the linear increase in de-alloyed fraction suggested by Fig. 9, is consistent with a process occurring on continuously renewed reactive surfaces.

4. Conclusions

An Au40Cu28Ag7Pd5Si20 alloy has been employed as test material for studying the de-alloying of amorphous alloys inthe form of a rapidly solidified ribbon. The potential must be chosen carefully following up potentiodynamic measurements to avoid extensive corrosion cracking. The de-alloying then occurs steadily throughout the ribbon conserving its pristine volume. The porous Au resulting from removal of alloying elements has uniform microstructure on both sides of the ribbon. Fine crystals are nucleated at the solid–electrolyte interface with random orientation. They then coarsen to give interconnected ligaments of larger size. The de-alloyed thickness increases linearly with time as determined by measuring the heat evolved during the crystallisation of the remaining amorphous phase suggesting the process occurs on continuously renewed reactive surfaces.

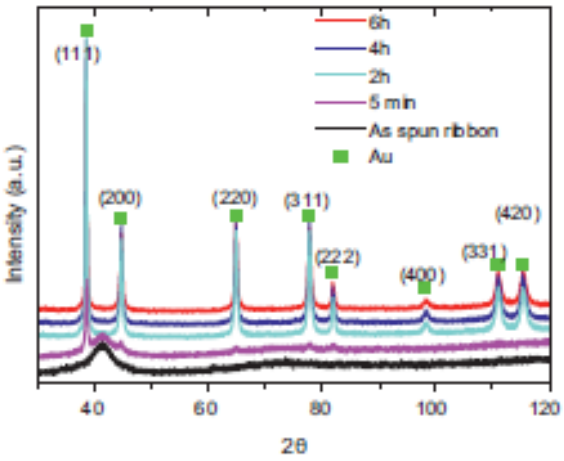

Fig. 1. XRD patterns given by the as-spun ribbon and de-alloyed samples for the times listed in the legend.

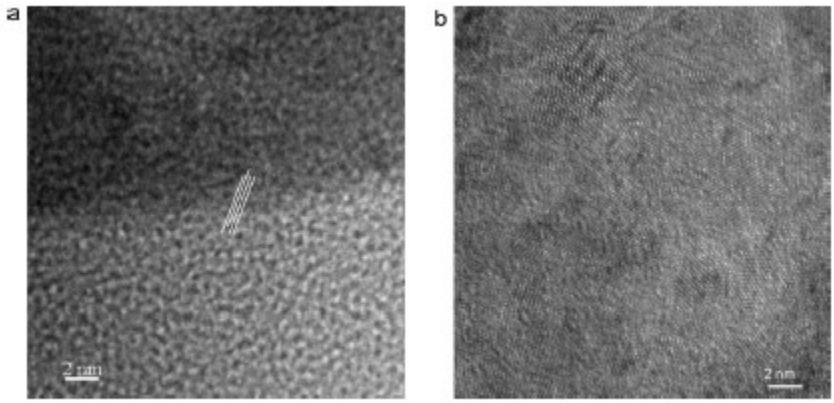

Fig. 2. High resolution TEM image of an as-spun ribbon (a) and a sample de-alloyed in 1 M HNO_3 at 70 °C for 60 s (b).

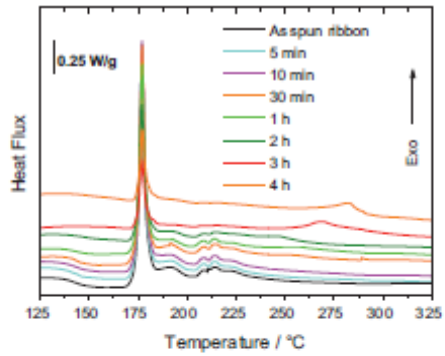

Fig. 3. DSC traces provided by de-alloyed samples for the times listed in the legend.

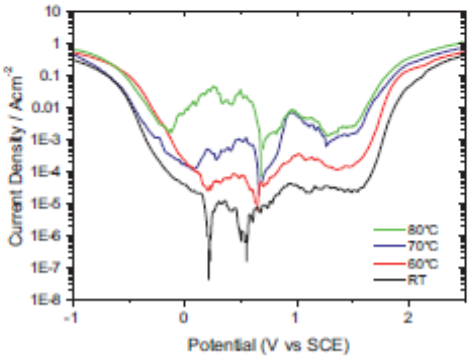

Fig. 4. Polarisation curves of the amorphous alloy obtained at various temperatures.

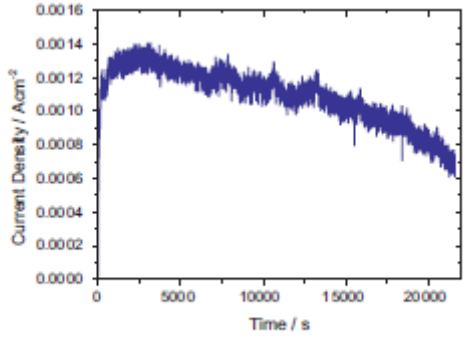

Fig. 5. Current vs time during potentiostatic de-alloying in 1 M HNO_3 at 70 °C (V vs).

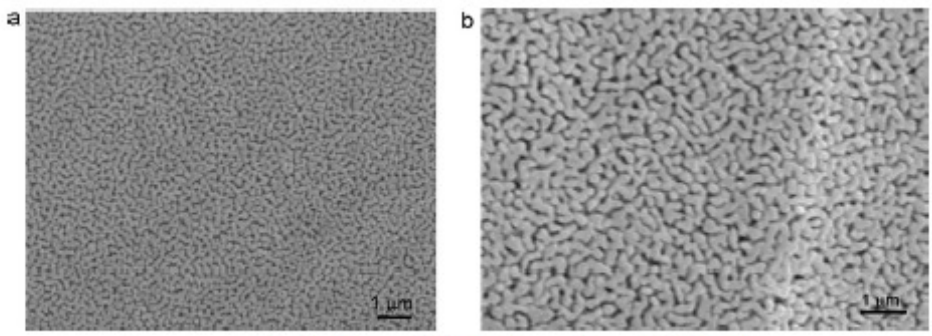

Fig. 6. SEM images of the surface of (a) a sample de-alloyed at for 600 s; (b) a sample de-alloyed at for 10,800 s.

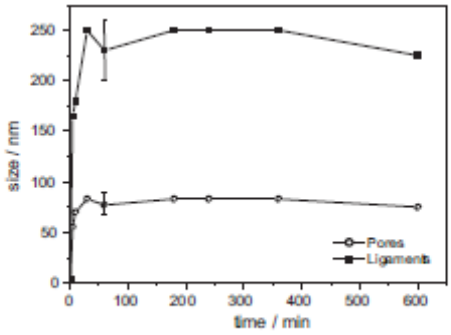

Fig. 7. The size of pores and ligaments as a function of de-alloying time.

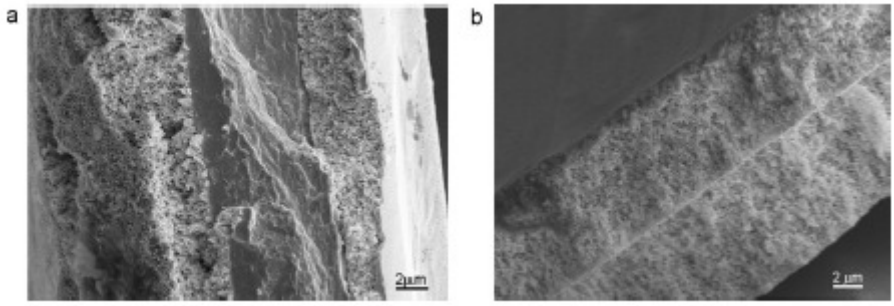

Fig. 8. SEM images of cross sections of ribbons after (a) partial (14,400 s) and (b) almost complete de-alloying (21,600 s).

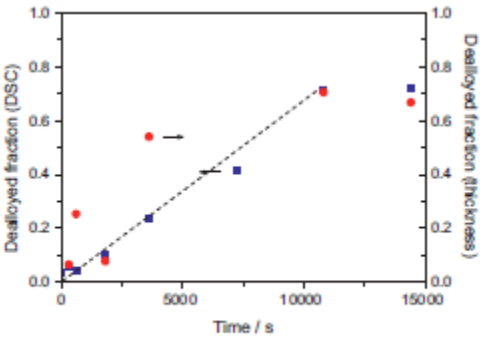

Fig. 9. The de-alloyed fraction as a function of time as derived from the crystallisation peaks reported in Fig. 3.

Acknowledgements

Work performed for MIUR-Progetto di Rilevante Interesse Nazionale 2008. Fondazione S. Paolo is acknowledged for support to CdE NIS.

References

[1] J. Erlebacher, R. Seshadri (Eds.), MRS Bull. 34 (2009).
[2] J.D. Fritz, H.W. Pickering, J. Electrochem. Soc. 138 (11) (1991) 3209–3218.
[3] X. Lu, E. Bischoff, R. Spolenak, T.J. Balk, Scr. Mater. 56 (2007) 557–560.
[4] J. Erlebacher, M.J. Aziz, A. Karma, N. Dimitov, K. Sieradzki, Nature 410 (2001) 450–453.
[5] S. Van Petegem, S. Brandstetter, R. Maass, A.M. Hodge, B.S. El-Dasher, J. Biener, B. Schmitt, C. Borca, H. Van Swygenhoven, Nano Lett. 9 (2009) 1158–1163.
[6] J.C. Thorp, K. Sieradzki, L. Tang, P.A. Crozier, A. Misra, M. Nastasi, D. Mitlin, S.T. Picraux, Appl. Phys. Lett. 88 (2006) 033110.
[7] J. Yu, Y. Ding, C. Xu, A. Inoue, T. Sakurai, M. Chen, Chem. Mater. 20 (2008) 4548–4550.
[8] H. Abe, K. Sato, H. Nishikawa, T. Takemoto, M. Fukuhara, A. Inoue, Mater. Trans. 50 (2009) 1255–1258.
[9] J. Jayarai, J.M. Park, P.F. Gostin, E. Fleury, A. Gebert, L. Schultz, Intermetallics 17 (2009) 1120–1123.
[10] F. Scaglione, A. Gebert, L. Battezzati, Intermetallics 18 (2010) 2338–2342.
[11] L. Battezzati, F. Scaglione, J. Alloys Compd. 509S (2011) S8–S12.
[12] H. Guo, W. Zhang, C. Qin, J. Qiang, M. Chen, A. Inoue, Mater. Trans. 50 (2009) 1290–1293.
[13] H.W. Pickering, Corros. Sci. 23 (1983) 1107–1120.
[14] L. Lutterotti, S. Matthies, H.-R. Wenk, MAUD (Material Analysis Using Diffraction) is released under free license of the authors. Available at: http://www.ing.unitn.it/wmaud/index.html.